

248 nm. From a calibration of the fluorescence intensities using the 193-nm photolysis of HNO<sub>3</sub> and CH<sub>3</sub>ONO, respectively, the quantum yields of OH and CH<sub>3</sub>O formation can be determined as

$$\varphi(\text{OH}) = \Delta[\text{OH}]/\Delta[\text{CH}_3\text{O}_2] = 0.06 \pm 0.03$$

$$\varphi(\text{CH}_3\text{O}) = \Delta[\text{CH}_3\text{O}]/\Delta[\text{CH}_3\text{O}_2] = 0.2 \pm 0.1$$

where  $\Delta[\text{CH}_3\text{O}_2]$  represents the amount of CH<sub>3</sub>O<sub>2</sub> dissociated per 248-nm laser pulse. The error limits are estimates based on the accuracies of the laser pulse energy measurements ( $\pm 15\%$ ) and the accuracies of the absorption coefficients ( $\pm 10\%$ ).

The concentrations OH and CH<sub>3</sub>O observed prior to the 248-nm pulse are the result of a reaction of hot CH<sub>3</sub> radicals, generated in the 193-nm photolysis of azomethane, with O<sub>2</sub>.<sup>10</sup> The amount of CH<sub>3</sub> lost in these channels relative to CH<sub>3</sub>O<sub>2</sub> formation can also be estimated from the calibrated fluorescence intensities. We obtain 0.55% and 2.7% for OH and CH<sub>3</sub>O, respectively.

These figures clearly exclude the possibility that the increase of OH and CH<sub>3</sub>O observed after the 248-nm pulse is also due to a reaction of hot CH<sub>3</sub> with O<sub>2</sub>. With the ratio of the optical densities  $[\text{AM}]\sigma_{\text{AM}}^{193}/[\text{CH}_3\text{O}_2]\sigma_{\text{CH}_3\text{O}_2}^{248} \approx 12$  and a typical ratio of the laser photon densities of  $N_p^{193}/N_p^{248} \approx 0.5$  the total concentration of photofragments from CH<sub>3</sub>O<sub>2</sub> can at best be  $\sim 10\%$  that from azomethane ( $\sim 3 \times 10^{11} \text{ cm}^{-3}$  vs  $3 \times 10^{12} \text{ cm}^{-3}$ ). As a consequence we would expect a correspondingly small increase of the OH and CH<sub>3</sub>O signals even with unit quantum yield for CH<sub>3</sub> formation.

The sum of the quantum yields of OH and CH<sub>3</sub>O formation reflects the total quantum yield for O-O bond cleavage in the 248

nm photolysis of CH<sub>3</sub>O<sub>2</sub>. From mass balance considerations we then conclude that the dominant products ( $74 \pm 13\%$ ) of the photodissociation are CH<sub>3</sub> + O<sub>2</sub>. The correlation diagram of Figure 4 suggests that the O<sub>2</sub> product must be formed in the excited ( $a^1\Delta_g$ ) state. Since the quenching of O<sub>2</sub>( $a^1\Delta_g$ ) by O<sub>2</sub> is relatively inefficient ( $k = 2 \times 10^{-18} \text{ cm}^3 \text{ s}^{-1}$ )<sup>12</sup> emission from this state should be observable. However, in view of the low concentrations expected ( $\sim 2 \times 10^{11} \text{ cm}^{-3}$ ) we have not attempted this experiment.

The photodissociation of CH<sub>3</sub>O<sub>2</sub> in its first UV band has to our knowledge not been investigated before. Compared to the photodissociation of HO<sub>2</sub>, however, there appears to be a distinct modification in the product routes. Whereas for HO<sub>2</sub> the dominant products are OH( $X^2\Pi$ ) + O( $^1D$ ),<sup>4,6</sup> the corresponding channel for CH<sub>3</sub>O<sub>2</sub>, namely CH<sub>3</sub>O( $\tilde{X}^2E$ ) + O, only accounts for  $20 \pm 10\%$ . The dominant photodissociation channel of CH<sub>3</sub>O<sub>2</sub>, namely O<sub>2</sub> elimination, is apparently prevented for HO<sub>2</sub> due to the existence of a high barrier along this coordinate. Finally, formation of OH( $A^2\Sigma^+$ ), which for CH<sub>3</sub>O<sub>2</sub> is interpreted as a result of a complex dissociation pathway, is endothermic for HO<sub>2</sub> with 248-nm radiation and only accessible at  $\leq 190 \text{ nm}$ .

*Acknowledgment.* Financial support of this work by Deutsche Forschungsgemeinschaft (Sonderforschungsbereich 93, Schwerpunktsprogramm MAP) and by Fonds der Chemischen Industrie is gratefully acknowledged.

(12) Becker, K. H.; Groth, W.; Schurath, U. *Chem. Phys. Lett.* **1971**, *8*, 259.

## Decomposition of Propanal at Elevated Temperatures. Experimental and Modeling Study

Assa Lifshitz,\* Carmen Tamburu, and Aya Suslensky

Department of Physical Chemistry, The Hebrew University, Jerusalem 91904, Israel  
(Received: August 7, 1989; In Final Form: October 16, 1989)

The thermal decomposition of propanal (CH<sub>3</sub>CH<sub>2</sub>CHO) highly diluted in argon was studied behind reflected shocks in a pressurized-driver single-pulse shock tube over the temperature range 970–1300 K and overall densities of  $\sim 2.5 \times 10^{-3} \text{ mol/cm}^3$ . Under these conditions the following decomposition products were obtained (in order of decreasing abundance): CO, C<sub>2</sub>H<sub>4</sub>, CH<sub>4</sub>, C<sub>2</sub>H<sub>6</sub>, C<sub>3</sub>H<sub>8</sub>, C<sub>3</sub>H<sub>6</sub>, C<sub>4</sub>H<sub>6</sub>, and C<sub>2</sub>H<sub>2</sub>. Mixtures containing 0.1% propanal and 1% toluene in argon showed a factor of  $\sim 3$  decrease in the production rate of ethylene, indicating the involvement of a free-radical mechanism. Two dissociation reactions initiate the decomposition of propanal: (1) C<sub>2</sub>H<sub>5</sub>CHO  $\rightarrow$  C<sub>2</sub>H<sub>5</sub><sup>\*</sup> + CHO<sup>\*</sup> and (2) C<sub>2</sub>H<sub>7</sub>CHO  $\rightarrow$  CH<sub>3</sub><sup>\*</sup> + CH<sub>2</sub><sup>\*</sup>CHO. It then proceeds via a free-radical chain mechanism where the most important reactions are C<sub>2</sub>H<sub>5</sub>CHO + R<sup>\*</sup>  $\rightarrow$  CH<sub>3</sub>CH<sub>2</sub>CO<sup>\*</sup> + RH, CH<sub>3</sub>CH<sub>2</sub>CO<sup>\*</sup>  $\rightarrow$  C<sub>2</sub>H<sub>5</sub><sup>\*</sup> + CO, and CH<sub>3</sub>CH<sub>2</sub>CO<sup>\*</sup>  $\rightarrow$  CH<sub>3</sub><sup>\*</sup> + CH<sub>2</sub>CO. The overall decomposition of propanal was computer modeled with a reaction scheme containing 22 species and 52 elementary reactions. A sensitivity analysis showed that the system is very sensitive to the two initiation reactions and to the two-channel dissociation of the radical CH<sub>3</sub>CH<sub>2</sub>CO<sup>\*</sup>. The concentration ratio [C<sub>2</sub>H<sub>4</sub>]/[CH<sub>4</sub>] is highly dependent on  $k(\text{C}_2\text{H}_5+\text{CO})/k(\text{CH}_3+\text{CH}_2=\text{CO})$ . A ratio of  $\sim 100$  in the rate constants accounts for a ratio of  $\sim 30$  in the concentrations of ethylene and methane. There are four major free radicals in the system, C<sub>2</sub>H<sub>5</sub>, CH<sub>3</sub>, and H, and HCO. The modeling studies show that they reach steady-state concentrations after several hundred microseconds. The rate constant for the overall pyrolysis of propanal over the temperature and pressure ranges covered in this investigation is  $k_{\text{total}} = 10^{16.39} \exp(-73 \times 10^3/RT) \text{ s}^{-1}$ , where  $R$  is expressed in units of cal/(K mol).

### Introduction

One of the major reactions in the thermal decomposition of cyclic ethers is the isomerization to aldehydes and/or ketones. Crotonaldehyde (butenal) is a major product in the decomposition of 2,3-dihydrofuran<sup>1</sup> whereas ethylene oxide isomerizes to acetaldehyde.<sup>2,3</sup> Propionaldehyde (propanal) and acetone are the major products in the isomerization of propylene oxide.<sup>4-6</sup>

Whereas the decomposition of acetaldehyde has been thoroughly studied both at low and at high temperatures,<sup>7,8</sup> as far as we are aware only low-temperature studies of propanal pyrolysis have been reported.

(1) Lifshitz, A.; Bidani, M. *J. Phys. Chem.* **1989**, *93*, 1139.

(2) Setser, D. W. *J. Phys. Chem.* **1966**, *70*, 826.

(3) Lifshitz, A.; Ben-Hamou, H. *J. Phys. Chem.* **1983**, *87*, 1782.

(4) Hardwick, T. J. *Can. J. Chem.* **1968**, *46*, 2454.

(5) Blades, A. T. *Can. J. Chem.* **1968**, *46*, 3283.

(6) Flowers, M. C. *J. Chem. Soc., Faraday Trans. 1* **1977**, *73*, 1927.

(7) Colket III, M. B.; Nageli, D. W.; Glassman, I. *Int. J. Chem. Kinet.* **1975**, *7*, 223.

(8) Lepout, M. *J. Chim. Phys.* **1937**, *34*, 206.

The decomposition of propanal was reported in a series of articles by G. Ács et al.<sup>9-11</sup> The authors used a static system and covered the temperature range 696–823 K at pressures ranging between 50 and 200 Torr. In a series of articles describing the decomposition of propanal in the presence of various additives, the authors determined power and temperature dependences for the production of the different reaction products. The major reaction products of the decomposition were carbon monoxide and ethane. Ethylene and methane appeared in considerably lower concentrations and propylene and butane in very small quantities.<sup>9</sup>

The [ethane]/[ethylene] ratio in the pyrolysis is determined by the ratio of the rates of abstraction to decomposition of ethyl radicals. This ratio is strongly temperature dependent. It is therefore expected that this ratio and other features of the pyrolysis pattern will change at higher temperatures.

This article presents part of a continuous effort in this laboratory to investigate the thermal reactions of cyclic ethers and their decomposition and isomerization products. It describes an investigation of propanal pyrolysis over the temperature range 970–1350 K, using the single-pulse shock-tube technique. It provides a detailed account of the product distribution over the entire temperature range and compares the experimental results to those of computer modeling by using a reaction scheme with 22 species and 52 elementary steps.

### Experimental Section

**Apparatus.** The decomposition of propanal was studied behind reflected shock waves using the single-pulse shock-tube technique. The tube was made of 52-mm-i.d. electropolished stainless steel tubing. The driven section was 4 m long, and the driver had a variable length up to a maximum of 2.7 m, which could be varied in small steps in order to tune for the best cooling conditions. A 36-L dump tank was connected to the driven section at 45° angle toward the driver, near the diaphragm holder, in order to prevent reflection of transmitted waves. The driven section was separated from the driver by "Mylar" polyester film of thickness ranging from 0.001 to 0.002 in. depending upon the desired shock strength. Prior to the experiment the tube was pumped down to approximately  $2 \times 10^{-5}$  Torr and was then filled with 80–120 Torr of the reaction mixture. After the shock was fired, gas samples were collected from the tube and were analyzed by gas chromatography using a flame ionization detector.

Reflected shock parameters were calculated from the measured incident shock velocities by using the three conservation equations and the ideal gas equation of state. The molar enthalpies of propanal were taken from Stull et al.<sup>12</sup> and were extrapolated to higher temperatures by use of the Wilhoit polynomials.<sup>13</sup>

Incident shock velocities were measured with two miniature, high-frequency pressure transducers (Vibrometer Model 6QP500) placed 300 mm apart near the end plate of the driven section. The signals generated by the shock wave passing over the transducers were fed through a piezo amplifier to a Nicolet Model 3091 digital oscilloscope. Time intervals between the two signals shown on the oscilloscope were obtained digitally with an accuracy of 2  $\mu$ s corresponding to a temperature uncertainty of 10–15 K depending upon the shock temperature. A third transducer (P.C.B. Model 113A26) placed at the center of the end plate provided measurements of the reaction dwell times (approximately 2 ms) with an accuracy of  $\sim 5\%$ . Cooling rates were approximately  $5 \times 10^5$  K/s.

A more detailed description of the tube and its mode of operation have been described in previous publications.<sup>14</sup>

**Materials and Analysis.** Reaction mixtures containing 1% propanal in argon were prepared manometrically and stored at

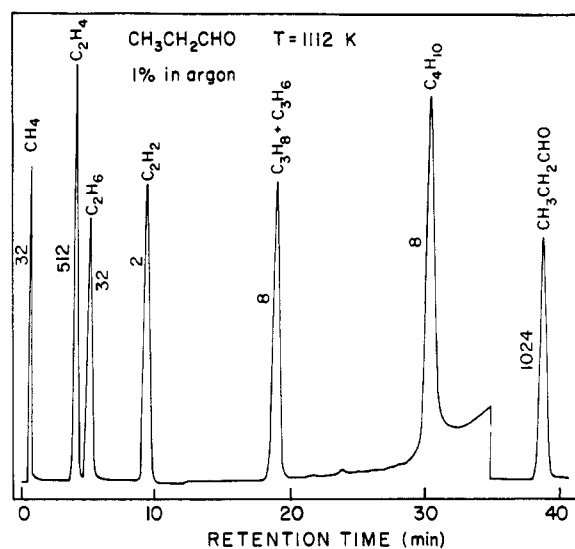


**Figure 1.** Gas chromatogram of a post-shock mixture of 1% propanal in argon heated to 1112 K, obtained on a 2-m Porapak N column using FID. Carbon monoxide which is analyzed in a separate run is not shown. (The numbers on the peaks indicate relative attenuation factors.)

a pressure of 1 atm in 12-L glass bulbs. Both the bulbs and the vacuum line were pumped down to less than  $10^{-5}$  Torr before the preparation of the mixtures.

Propanal, listed as 99%, pure was obtained from Aldrich Chemical Company Inc. None of the reaction products were found in the original material. Argon was Matheson ultra-high-purity grade, listed as 99.9995%, and helium was Matheson pure grade, listed as 99.999%. All materials were used without further purification.

The gas chromatographic analysis of the postshock mixtures was performed on two columns. The analysis of all the products except for CO was performed on a 2-m Porapak N column. Its initial temperature of 35 °C was gradually elevated to 150 °C in an analysis that lasted about 1 h. Carbon monoxide was analyzed on a room temperature 2-m molecular sieve 5A column. It was reduced at 400 °C to methane prior to its detection using a Chrompak methanizer with a carrier composed of 50% hydrogen and 50% argon. This analysis gave the ratio  $[CO]/[CH_4]$ . From this ratio and the known methane concentration obtained in the Porapak N analysis, the concentration of CO could be calculated. The ratio  $[CO]/[CH_4]$  in a standard mixture of methane and carbon monoxide was determined periodically in order to verify complete conversion of the latter to methane in the methanizer. A typical chromatogram of a shocked mixture of 1% propanal in argon heated to 1185 K is shown in Figure 1.

GC peak areas were integrated with a Spectra Physics Model SP4200 computing integrator and were transferred to a C.D.C. CYBER 180/855 main frame computer for data reduction and graphical presentations.

### Experimental Results

**Evaluation of Product Concentrations.** Product concentrations were evaluated from their GC peak areas in the following manner:

1. The concentration of propanal behind the reflected shock prior to decomposition,  $C_5(\text{propanal})_0$ , is given by

$$C_5(\text{propanal})_0 = \{p_1[\%(\text{propanal})]\rho_5/\rho_1\}/100RT_1 \quad (\text{I})$$

where  $p_1$  is the pressure in the tube prior to shock heating,  $\%(\text{propanal})$  is the percent of propanal in the original mixture,  $\rho_5/\rho_1$  is the compression behind the reflected shock, and  $T_1$  is room temperature.

2. The concentration of propanal behind the reflected shock prior to decomposition in terms of its peak area,  $A(\text{propanal})_0$  is given by

$$A(\text{propanal})_0 = A(\text{propanal})_t + \frac{1}{3} \sum N(p_i) A(p_i)_t / S(p_i) \quad (\text{II})$$

(9) Ács, G.; Tóth, G.; Huhn, P. *Magy. Kem. Foly.* **1973**, *79*, 386.

(10) Ács, G.; Tóth, G.; Huhn, P. *Acta Chim. (Budapest)* **1974**, *82*, 411.

(11) Ács, G.; Tóth, G.; Huhn, P. *Acta Chim. (Budapest)* **1974**, *82*, 425.

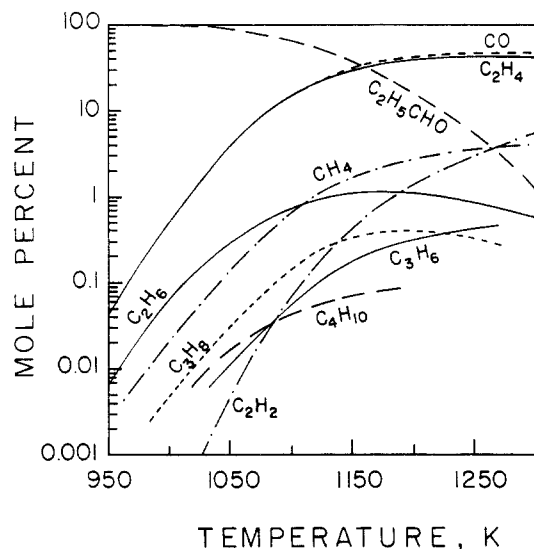
(12) Stull, D. R.; Westrum, Jr., E. F.; Sinke, G. C. *The Chemical Thermodynamics of Organic Compounds*; Wiley: New York, 1969.

(13) Wilhoit, R. C. *Thermodynamics Research Center Current Data News* Texas A&M University: College Station, 1975; Vol. 3, No. 2.

(14) Lifshitz, A.; Moran, A.; Bidani, S. *Int. J. Chem. Kinet.* **1987**, *19*, 61.

**TABLE I: Experimental Conditions and Product Distribution (mol %) in Representative Experiments**

T, K	$10^5 C_5$ , mol/cm <sup>3</sup>	CO	C <sub>2</sub> H <sub>4</sub>	C <sub>2</sub> H <sub>6</sub>	CH <sub>4</sub>	C <sub>2</sub> H <sub>2</sub>	C <sub>3</sub> H <sub>6</sub>	C <sub>3</sub> H <sub>8</sub>	C <sub>4</sub> H <sub>10</sub>	C <sub>2</sub> H <sub>5</sub> CHO
975	2.45	0.565	0.507	0.051	0.021					98.76
1005	2.55	1.21	1.10	0.091	0.104				0.003	97.49
1045	2.40	7.69	6.78	0.462	0.264		0.032			84.77
1085	3.11	23.8	26.9	1.29	1.36	0.049	0.064	0.257	0.081	46.16
1112	2.94	27.9	30.5	1.15	1.57	0.129	0.097	0.235	0.056	38.32
1165	2.73	40.7	38.8	1.20	2.58	0.685	0.248	0.383	0.097	15.07
1220	2.38	46.1	42.4	1.132	3.78	2.19	0.363	0.381	0.031	3.74
1270	2.15	50.8	38.0	1.00	4.70	2.76	0.370	0.204	0.022	1.02

**Figure 2.** Distribution of reaction products as obtained in the post-shock analyses. Ethylene and carbon monoxide are the major products.

where  $A(\text{propanal})_i$  is the peak area of propanal in the shocked sample,  $A(\text{pr}_i)_i$  is the peak area of a product  $i$  in the shocked sample,  $S(\text{pr}_i)$  is its sensitivity relative to propanal, and  $N(\text{pr}_i)$  is the number of its carbon atoms.

In tests where the shock temperature is low and the conversion is small,  $C_5(\text{propanal})_0 \approx C_5(\text{propanal})_i$ , and the second term in the right-hand side of eq II which gives the amount of propanal decomposed is a second-order correction. When high conversions are concerned, the second term is important.

3. The concentration of a product  $i$  in the shocked sample is given by

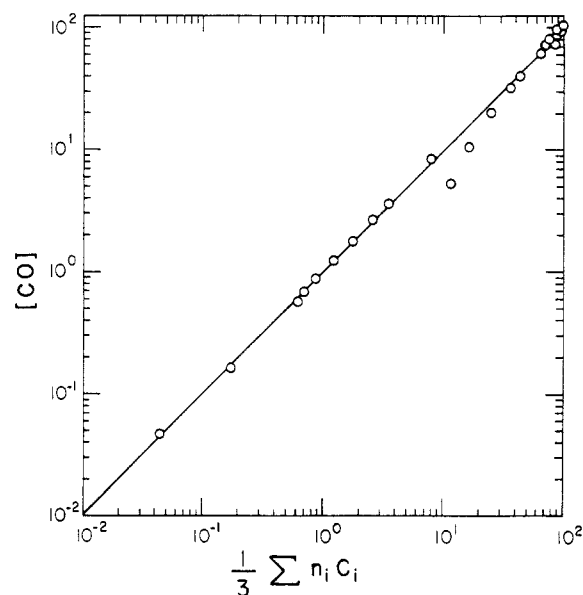
$$C_5(\text{pr}_i)_i = [A(\text{pr}_i)_i / S(\text{pr}_i)] \{ C_5(\text{propanal})_0 / A(\text{propanal})_0 \} \quad (\text{III})$$

Since  $A(\text{propanal})_0$  is not available in the postshock analysis (only  $A(\text{propanal})_i$  is), its value is calculated from eq II.

**Product Distribution.** In order to determine the distribution of reaction products, tests were run with mixtures containing 1% propanal in argon, covering the temperature range 970–1350 K. Extents of pyrolysis as low as a few hundredths of one percent were determined.

Details of the experimental conditions and the distribution of reaction products in several representative tests are given in Table I. The table shows the temperature behind the reflected shock  $T_5$ , the overall density behind the reflected shock  $C_5$  (in units of mol/cm<sup>3</sup>), and the mole percent of the various reaction products in the mixture as obtained in the postshock analyses (not including hydrogen and argon). The concentration of propanal behind the reflected shock prior to decomposition  $\{C_5(\text{propanal})_0\}$  is given by the percent of propanal in the unshocked mixture times  $C_5$ . The percent of a given product in the total sample, as shown in Table I, corresponds to its mole fraction,  $(100C_i / \sum C_i)$  irrespective of the number of carbon atoms it contains.

Figure 2 shows the product distribution obtained in the postshock mixtures over the temperature range covered in this investigation. As can readily be seen, carbon monoxide and ethylene are the major reaction products and appear in almost equal concentrations. Methane and ethane concentrations are by a factor of approximately 50 lower, and acetylene, propylene, propane,

**Figure 3.** Plot of the concentration of carbon monoxide [CO] (the only oxygen-containing product) vs one-third the sum of the concentrations of all the products each multiplied by the number of its carbon atoms,  $1/3 \sum (n_i C_i)$ . A complete oxygen-carbon atom balance is maintained over the entire temperature range.

and butane appear in very low concentrations.

**Oxygen-Carbon Balance.** The balance of oxygen vs carbon among the decomposition products is shown in Figure 3. The concentrations of carbon monoxide [CO] (the only oxygen-containing product found in the postshock analyses) are plotted against one-third the sum of the concentrations of all the products each multiplied by the number of its carbon atoms,  $1/3 \sum (n_i C_i)$ , where  $n_i$  is the number of carbon atoms in a species  $i$  and  $C_i$  is the concentration of a species  $i$ . One-third is the ratio of oxygen to carbon atoms in the reactant molecule. The 45° line in the Figure represents a complete mass balance. As can be seen, oxygen-carbon balance is maintained over the entire temperature range of the investigation.

**Inhibited Reaction.** To assess the extent of free-radical reactions in the overall decomposition, several tests were run in the presence of a large excess of a free-radical scavenger. Production rates of ethylene (the major product in propanal pyrolysis) in mixtures containing 0.1% propanal in argon were compared to the rates in mixtures containing 0.1% propanal and 1% toluene.

The results of this series of experiments are shown in Figure 4 where the logarithm of the first-order rate constant for the formation of ethylene is plotted against reciprocal temperature. As can readily be seen the production rate of ethylene is reduced by a factor of approximately 3, indicating that free-radical reactions play an important role in the decomposition of propanal.

In this series of experiments we used the decomposition of 1-chloropropane to C<sub>3</sub>H<sub>6</sub> and HCl as a chemical thermometer in order to evaluate the reflected shock temperatures. 1-Chloropropane (0.1%) was added to the reaction mixtures, and the temperature was evaluated from ratios  $[C_3H_6] / \{ [CH_2ClCH_2CH_3] + [C_3H_6] \}$  in the shocked samples. (The amount of propylene formed by the decomposition of propanal under the condition of the experiment is negligible compared to the amount formed in the unimolecular decomposition of 1-

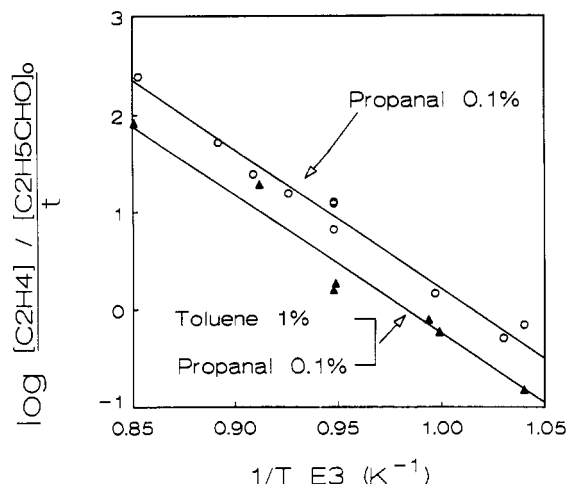


**Figure 4.** Plot of the logarithm of the first-order rate constant for the formation of ethylene vs reciprocal temperature. The production rate of ethylene is reduced by a factor of approximately 3.5 with excess toluene present, indicating the involvement of a free-radical mechanism.

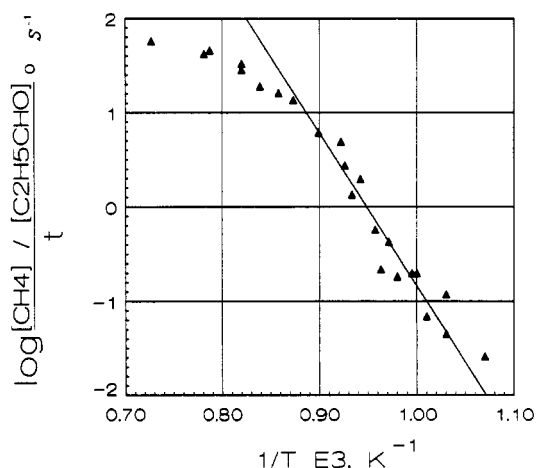


**Figure 5.** Production of methane. The points on the straight line correspond to a first-order rate constant from which Arrhenius parameters can be evaluated.

chloropropane). We used for the decomposition of 1-chloropropane the rate constant<sup>15</sup>  $k = 10^{12.98} \exp(-52.92 \times 10^3/RT) \text{ s}^{-1}$ .

**Arrhenius Parameters.** In Figure 5, as an example, the rate of production of methane defined as

$$\text{rate}(\text{methane}) = C_5(\text{methane})_t/t \quad (\text{IV})$$

and divided by the initial propanal concentration is plotted against reciprocal temperature. It is expressed in units of  $\text{s}^{-1}$  and at low extents of reaction resembles a first-order rate constant. As can be seen, the line bends as it approaches the high-temperature end. There are several reasons for such bends in plots of this type. Since the overall decomposition of propanal is a complex reaction, neither the disappearance of the reactant nor the production of any of the reaction products obeys a simple first-order relation. The only way to evaluate a first-order rate constant is by calculating a pseudo-zero-order constant and dividing it by the initial propanal concentration. This will be a good approximation as long as  $[\text{propanal}]_t \approx [\text{propanal}]_0$ . At high conversions and therefore at high temperatures this condition is not fulfilled and the evaluation of the rate constant is incorrect. Rate constants are underestimated at high temperatures causing bends in the  $\log k$  vs  $1/T$  plots. An additional reason for the curvature is the temperature drop during the course of the reaction owing to the endothermicity of the overall decomposition, which will be more

**TABLE II: Preexponential Factors ( $A$ ) and Activation Energies ( $E$ ) for the First-Order Rate Constants of Formation of Various Reaction Products**

product	$\log A, \text{ s}^{-1}$	$E, \text{ kcal/mol}$	$T, \text{ K}$
propanal <sup>a</sup>	16.39	73	950–1075
CO	16.77	75	970–1110
$\text{C}_2\text{H}_4$	16.70	75	970–1110
$\text{CH}_4$	15.52	75	970–1150
$\text{C}_2\text{H}_6$	14.51	69	970–1090
$\text{C}_2\text{H}_2$	18.81	98	1040–1220
$\text{C}_3\text{H}_8$	12.79	65	970–1160
$\text{C}_3\text{H}_6$	13.40	70	970–1150

<sup>a</sup> First-order rate constant for the overall decomposition of propanal.

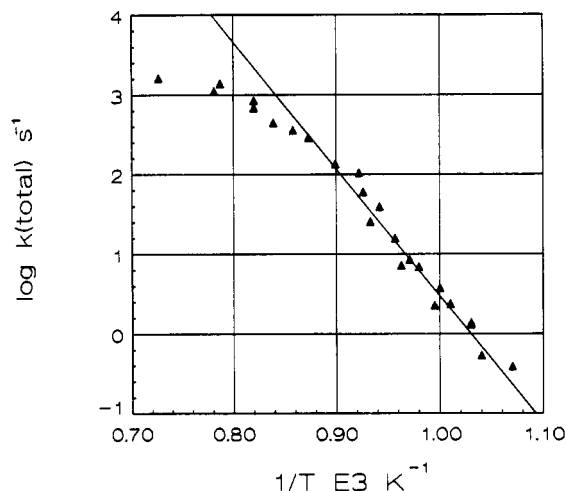


**Figure 6.** First-order rate constant for the overall decomposition of propanal, calculated from the relation  $k_{\text{total}} = -\ln \{[\text{propanal}]_t/[\text{propanal}]_0\}/t$ .

pronounced at high conversions (high temperatures).

Values of  $E$  in units of kcal/mol as obtained from the slopes of the lines and their corresponding preexponential factors are summarized in Table II. All were obtained from the low-temperature–low-conversion range in the figures before the curvature begins.

The parameters do not necessarily represent elementary unimolecular reactions. They simply offer a useful way to represent the experimental data.

Figure 6 shows the first-order rate constant for the overall decomposition of propanal,  $k_{\text{total}} = -\ln \{[\text{propanal}]_t/[\text{propanal}]_0\}/t$ . The value obtained is  $k_{\text{total}} = 10^{16.39} \exp(-73 \times 10^3/RT) \text{ s}^{-1}$ , where  $R$  is expressed in units of cal/(K mol). Again, the first-order rate constant does not imply that the decomposition reaction of propanal under the conditions studied is a simple unimolecular process. Instead, as will be discussed later, the decomposition is composed of a large number of elementary reactions involving unimolecular dissociations as well as free-radical reactions.

## Discussion

**Computer Modeling.** A reaction scheme containing 22 species and 52 elementary reactions was composed for the decomposition of propanal (Table III). Columns 2–4 in the table show the components of the forward rate constant (corrected for falloff effects where applicable) as the reaction is listed. Column 5 gives the values of the forward rate constant as calculated from the rate parameters for the temperature of 1000 K, and column 6 shows the value of the reverse rate constant calculated from  $k_f$  and the equilibrium constant of the reaction also at 1000 K. The scheme is composed of unimolecular dissociations of the reactant molecule, unimolecular dissociations of radical intermediates, abstractions, and recombinations. Rate parameters including falloff corrections were taken from the compilations of Tsang and Hampson<sup>16</sup> and of Warnatz.<sup>17</sup> They were varied within the limits of their reported

(15) Evans, P. J.; Ichimura, T.; Tschikow-Roux, E. *Int. J. Chem. Kinet.* **1978**, *10*, 855.

(16) Tsang, W.; Hampson, R. F. *J. Phys. Chem. Ref. Data* **1986**, *15*, 1087.

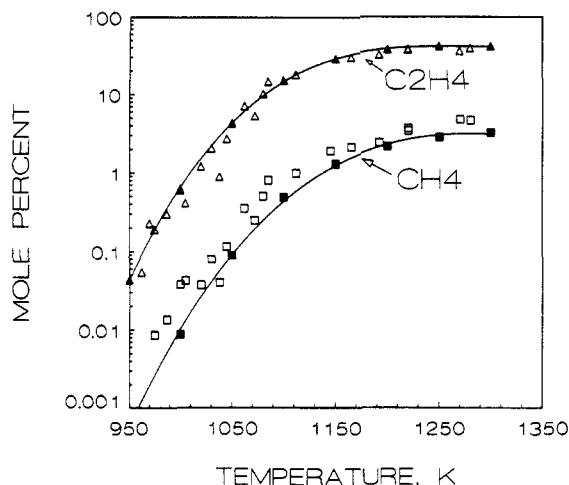


**Figure 7.** Comparison between experimental ( $\square$ ,  $\Delta$ ) and calculated ( $\blacksquare$ ,  $\blacktriangle$ ) mole percent of ethylene and methane.

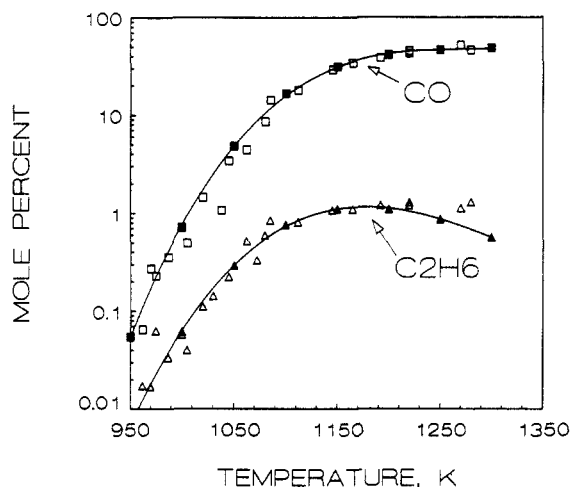


**Figure 8.** Comparison between experimental ( $\square$ ,  $\Delta$ ) and calculated ( $\blacksquare$ ,  $\blacktriangle$ ) mole percent of carbon monoxide and ethane.

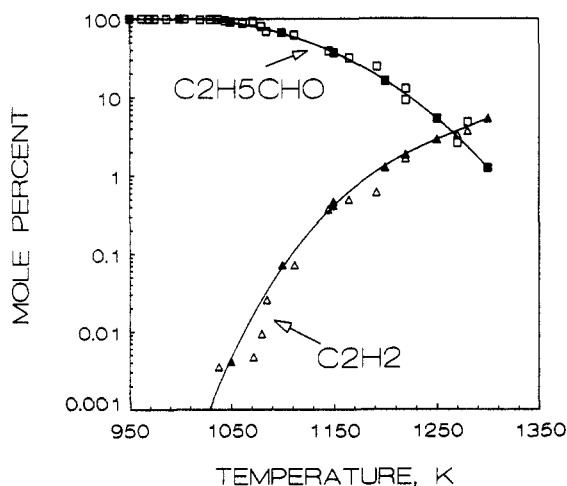


**Figure 9.** Comparison between experimental ( $\square$ ,  $\Delta$ ) and calculated ( $\blacksquare$ ,  $\blacktriangle$ ) mole percent of propanal and acetylene.

uncertainties. Parameters for reactions that could not be found in available compilations were estimated by comparison to similar reactions. The rate parameters for reactions 1, 16, 25, and 26, which were evaluated from the results of the modeling studies, will be discussed later.

Figures 7–9 show comparisons between mole percent of several products based on analyses of postshock mixtures and on calcu-

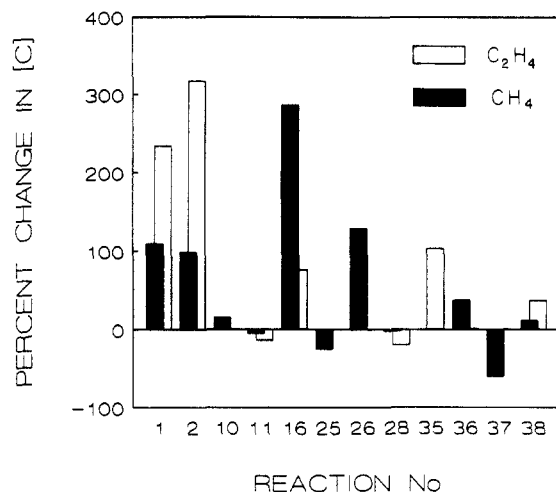


**Figure 10.** Sensitivity analysis for  $T_5 = 970$  K. Percent change in the concentrations of ethylene and methane due to a factor of 5 increase in the forward and reverse rate constants.

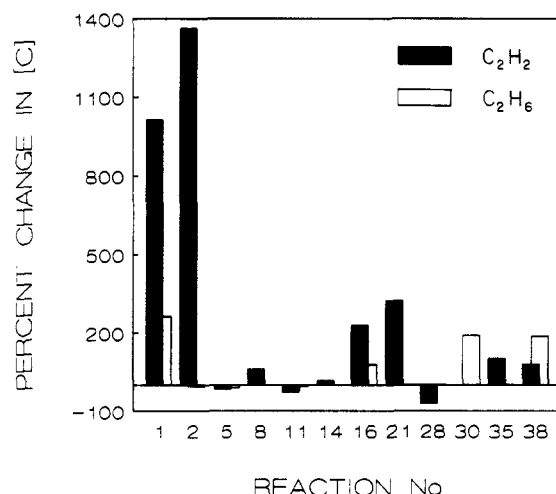


**Figure 11.** Sensitivity analysis for  $T_5 = 970$  K. Percent change in the concentration of ethane and acetylene due to a factor of 5 increase in the forward and reverse rate constants.

lations using the reaction scheme given in Table III and the experimentally determined reaction times. The open symbols on the figures are experimental points, and the solid line is the best fit through seven calculated points (filled symbols) at 50 K intervals. The agreement for the six species shown on the figures seems to be satisfactory.

Figures 10 and 11 show the sensitivity analysis for the formation of carbon monoxide, ethylene, methane, and ethane, calculated at 970 K. They show percent change in the concentration of a given product due to a factor of 5 increase in the forward and reverse rate constants. The figures concentrate on reactions that have the most influence on the production rates of these species.

**Reaction Mechanism and Discussion of Specific Reactions.** As a molecule with two C–C bonds of approximately equal strength, propanal dissociates in two dissociation channels, producing  $C_2H_5$  and  $HCO$  (reaction 1) and  $CH_3$  and  $CH_2CHO$  (reaction 16). Each of these four radicals enter into secondary reactions which fall into the categories of dissociations and abstractions (and some, mostly very slow, recombinations). The competition between these categories of elementary reactions is the main factor determining the distribution of reaction products.

As has already been shown, the concentrations of ethylene in the postshock mixtures are higher than those of methane by a factor of  $\sim 30$ . In order to reproduce this observation in the modeling experiments, we first assigned approximately the same ratio to the rate constants  $k_1$  and  $k_{16}$ . These two rate constants determine the rates at which ethyl and methyl radicals are formed in the initiation processes. Such an assignment could not generate the

(17) Warnatz, J. In *Combustion Chemistry*; Gardiner, W. C., Jr., Ed.; Springer-Verlag: Berlin, 1984; p 197.

TABLE III: Reaction Scheme<sup>a</sup>

reaction	A	n	E	k <sub>f</sub> <sup>b,c</sup>	k <sub>r</sub> <sup>b,d</sup>
(1) C <sub>2</sub> H <sub>5</sub> CHO → C <sub>2</sub> H <sub>5</sub> + HCO	0.725E+17	0	82 400	0.712E-01	0.167E+14
(2) C <sub>2</sub> H <sub>5</sub> → C <sub>2</sub> H <sub>4</sub> + H	0.480E+09	1.19	37 205	0.132E+05	0.150E+13
(3) C <sub>2</sub> H <sub>5</sub> + CH <sub>3</sub> → C <sub>3</sub> H <sub>8</sub>	0.245E+15	-0.5	0	0.774E+13	0.733E-02
(4) C <sub>2</sub> H <sub>5</sub> + CH <sub>3</sub> → CH <sub>4</sub> + C <sub>2</sub> H <sub>4</sub>	0.980E+13	-0.5	0	0.309E+12	0.453E-01
(5) C <sub>2</sub> H <sub>5</sub> + C <sub>2</sub> H <sub>5</sub> → C <sub>4</sub> H <sub>10</sub>	0.200E+13	0	0	0.200E+13	0.991E-02
(6) C <sub>2</sub> H <sub>5</sub> + HCO → C <sub>2</sub> H <sub>6</sub> + CO	0.120E+15	0	0	0.120E+15	0.180E-01
(7) C <sub>2</sub> H <sub>5</sub> + H → C <sub>2</sub> H <sub>4</sub> + H <sub>2</sub>	0.181E+13	0	0	0.181E+13	0.128E-01
(8) C <sub>2</sub> H <sub>5</sub> + C <sub>2</sub> H <sub>4</sub> → C <sub>2</sub> H <sub>6</sub> + C <sub>2</sub> H <sub>3</sub>	0.632E+03	3.13	18 011	0.179E+09	0.318E+11
(9) C <sub>2</sub> H <sub>5</sub> + H → C <sub>2</sub> H <sub>6</sub>	0.486E+13	0	0	0.486E+13	0.153E-06
(10) C <sub>2</sub> H <sub>5</sub> + H → CH <sub>3</sub> + CH <sub>3</sub>	0.168E+14	0	0	0.168E+14	0.350E+10
(11) C <sub>2</sub> H <sub>5</sub> + C <sub>2</sub> H <sub>5</sub> → C <sub>2</sub> H <sub>4</sub> + C <sub>2</sub> H <sub>6</sub>	0.400E+13	0	0	0.400E+13	0.143E+02
(12) CH <sub>4</sub> → CH <sub>3</sub> + H	0.780E+15	0	103 826	0.159E-07	0.124E+14
(13) CH <sub>3</sub> + CH <sub>3</sub> → C <sub>2</sub> H <sub>6</sub>	0.680E+15	-0.64	0	0.817E+13	0.124E-02
(14) CH <sub>3</sub> + C <sub>2</sub> H <sub>4</sub> → C <sub>2</sub> H <sub>3</sub> + CH <sub>4</sub>	0.662E+01	3.70	9 499	0.699E+10	0.505E+11
(15) CH <sub>3</sub> + C <sub>2</sub> H <sub>4</sub> → <i>n</i> -C <sub>3</sub> H <sub>7</sub>	0.331E+12	0	7 705	0.685E+10	0.256E+07
(16) C <sub>2</sub> H <sub>5</sub> CHO → CH <sub>2</sub> CHO + CH <sub>3</sub>	0.478E+17	0	84 000	0.210E-01	0.250E+14
(17) HCO + Ar → H + CO + Ar	0.511E+22	-2.14	20 425	0.669E+11	0.318E+15
(18) HCO + H → H <sub>2</sub> + CO	0.120E+15	0	0	0.120E+15	0.355E-04
(19) C <sub>2</sub> H <sub>3</sub> + CH <sub>2</sub> O → C <sub>2</sub> H <sub>4</sub> + HCO	0.542E+04	2.81	50 000	0.172E+02	0.122E-02
(20) H <sub>2</sub> + Ar → H + H + Ar	0.457E+20	-1.40	104 391	0.444E-07	0.715E+15
(21) H + C <sub>2</sub> H <sub>4</sub> → C <sub>2</sub> H <sub>3</sub> + H <sub>2</sub>	0.663E+06	2.53	12 242	0.544E+11	0.190E+11
(22) H + C <sub>2</sub> H <sub>3</sub> → C <sub>2</sub> H <sub>2</sub> + H <sub>2</sub>	0.963E+14	0	0	0.963E+14	0.616E+00
(23) CH <sub>2</sub> CHO → CH <sub>2</sub> CO + H	0.200E+14	0	37 000	0.164E+06	0.266E+13
(24) C <sub>2</sub> H <sub>4</sub> CHO → C <sub>2</sub> H <sub>4</sub> + HCO	0.800E+14	0	20 000	0.340E+10	0.106E+13
(25) C <sub>2</sub> H <sub>5</sub> + CO → C <sub>2</sub> H <sub>5</sub> CO	0.375E+11	0	4 809	0.333E+10	0.167E+10
(26) C <sub>2</sub> H <sub>5</sub> CO → CH <sub>3</sub> + CH <sub>2</sub> CO	0.800E+14	0	30 000	0.222E+08	0.764E+12
(27) C <sub>2</sub> H <sub>3</sub> + Ar → C <sub>2</sub> H <sub>2</sub> + H + Ar	0.231E+42	-7.49	45 542	0.873E+09	0.899E+17
(28) C <sub>2</sub> H <sub>5</sub> CHO + H → C <sub>2</sub> H <sub>5</sub> CO + H <sub>2</sub>	0.554E+03	3.50	5 167	0.130E+13	0.453E+08
(29) C <sub>2</sub> H <sub>5</sub> CHO + CH <sub>3</sub> → C <sub>2</sub> H <sub>5</sub> CO + CH <sub>4</sub>	0.164E+01	4.0	8 285	0.254E+11	0.183E+08
(30) C <sub>2</sub> H <sub>5</sub> CHO + C <sub>2</sub> H <sub>5</sub> → C <sub>2</sub> H <sub>5</sub> CO + C <sub>2</sub> H <sub>6</sub>	0.225E+01	3.65	9 141	0.201E+10	0.356E+08
(31) C <sub>2</sub> H <sub>5</sub> CHO + HCO → C <sub>2</sub> H <sub>5</sub> CO + CH <sub>2</sub> O	0.470E+05	2.72	18 235	0.703E+09	0.985E+09
(32) C <sub>2</sub> H <sub>5</sub> CHO + C <sub>2</sub> H <sub>3</sub> → C <sub>2</sub> H <sub>5</sub> CO + C <sub>2</sub> H <sub>4</sub>	0.850E+10	0	6 000	0.415E+09	0.413E+05
(33) C <sub>2</sub> H <sub>5</sub> CHO + <i>n</i> -C <sub>3</sub> H <sub>7</sub> → C <sub>2</sub> H <sub>5</sub> CO + C <sub>3</sub> H <sub>8</sub>	0.843E-02	4.20	8 716	0.417E+09	0.520E+07
(34) C <sub>2</sub> H <sub>5</sub> CHO + <i>i</i> -C <sub>3</sub> H <sub>7</sub> → C <sub>2</sub> H <sub>5</sub> CO + C <sub>3</sub> H <sub>8</sub>	0.843E-02	4.20	8 716	0.417E+09	0.920E+07
(35) C <sub>2</sub> H <sub>5</sub> CHO + H → C <sub>2</sub> H <sub>4</sub> CHO + H <sub>2</sub>	0.184E+03	3.50	5 167	0.432E+12	0.229E+10
(36) C <sub>2</sub> H <sub>5</sub> CHO + CH <sub>3</sub> → C <sub>2</sub> H <sub>4</sub> CHO + CH <sub>4</sub>	0.164E+01	4.0	8 285	0.254E+11	0.279E+10
(37) C <sub>2</sub> H <sub>5</sub> CHO + CH <sub>3</sub> → C <sub>3</sub> H <sub>8</sub> + HCO	0.250E+13	0	9 000	0.269E+11	0.599E+10
(38) C <sub>2</sub> H <sub>5</sub> CHO + C <sub>2</sub> H <sub>5</sub> → C <sub>2</sub> H <sub>4</sub> CHO + C <sub>2</sub> H <sub>6</sub>	0.225E+01	3.65	9 141	0.201E+10	0.543E+10
(39) C <sub>2</sub> H <sub>5</sub> CHO + HCO → C <sub>2</sub> H <sub>4</sub> CHO + CH <sub>2</sub> O	0.470E+05	2.72	18 235	0.703E+09	0.150E+12
(40) C <sub>2</sub> H <sub>5</sub> CHO + C <sub>2</sub> H <sub>3</sub> → C <sub>2</sub> H <sub>4</sub> CHO + C <sub>2</sub> H <sub>4</sub>	0.850E+10	0	6 000	0.415E+09	0.631E+07
(41) C <sub>2</sub> H <sub>5</sub> CHO + <i>n</i> -C <sub>3</sub> H <sub>7</sub> → C <sub>2</sub> H <sub>4</sub> CHO + C <sub>3</sub> H <sub>8</sub>	0.843E-02	4.20	8 716	0.417E+09	0.794E+09
(42) C <sub>2</sub> H <sub>5</sub> CHO + <i>i</i> -C <sub>3</sub> H <sub>7</sub> → C <sub>2</sub> H <sub>4</sub> CHO + C <sub>3</sub> H <sub>8</sub>	0.843E-02	4.20	8 716	0.417E+09	0.140E+10
(43) CH <sub>3</sub> + C <sub>2</sub> H <sub>4</sub> → C <sub>3</sub> H <sub>6</sub> + H	0.200E+14	0	10 000	0.130E+12	0.464E+15
(44) CH <sub>4</sub> + H → CH <sub>3</sub> + H <sub>2</sub>	0.225E+05	3.0	8 756	0.274E+12	0.132E+11
(45) C <sub>2</sub> H <sub>6</sub> + H → C <sub>2</sub> H <sub>5</sub> + H <sub>2</sub>	0.554E+03	3.50	5 167	0.130E+13	0.256E+10
(46) CH <sub>3</sub> + C <sub>2</sub> H <sub>6</sub> → CH <sub>4</sub> + C <sub>2</sub> H <sub>5</sub>	0.548E+00	4.0	8 285	0.847E+10	0.345E+09
(47) <i>i</i> -C <sub>3</sub> H <sub>7</sub> → C <sub>3</sub> H <sub>6</sub> + H	0.892E+13	0	35 753	0.137E+06	0.230E+13
(48) <i>i</i> -C <sub>3</sub> H <sub>7</sub> + H <sub>2</sub> → C <sub>3</sub> H <sub>8</sub> + H	0.349E+03	3.28	8 670	0.307E+11	0.194E+14
(49) <i>n</i> -C <sub>3</sub> H <sub>7</sub> + H <sub>2</sub> → C <sub>3</sub> H <sub>8</sub> + H	0.181E+04	2.84	9 141	0.602E+10	0.215E+13
(50) HCO + H <sub>2</sub> → CH <sub>2</sub> O + H	0.181E+07	2.0	17 830	0.229E+09	0.924E+13
(51) <i>i</i> -C <sub>3</sub> H <sub>7</sub> + CH <sub>3</sub> → C <sub>4</sub> H <sub>10</sub>	0.137E+16	-0.68	0	0.124E+14	0.123E-01
(52) <i>i</i> -C <sub>3</sub> H <sub>7</sub> + CH <sub>3</sub> → CH <sub>4</sub> + C <sub>3</sub> H <sub>6</sub>	0.219E+15	-0.68	0	0.199E+13	0.431E-01

<sup>a</sup> In this table, 0.725E+17 represents  $0.725 \times 10^{17}$ . <sup>b</sup> Rate constants,  $k = AT^n \exp(-E/RT)$ , are expressed in units of  $\text{cm}^3 \text{s mol}^{-1}$ . <sup>c</sup> Forward rate constant at 1000 K. <sup>d</sup> Reverse rate constant at 1000 K.

above-mentioned ratio in ethylene to methane concentration. Any attempt to further increase this ratio resulted in serious disturbance in the predicted mole percent of almost all the other products. In addition, in order to reproduce the absolute mole percent of ethylene and methane, the preexponential factors of reactions 1 and 16 had to be assigned unrealistically high values. The reason for these results is that reaction 1 is not the main supplier of ethyl radicals. The intermediate species C<sub>2</sub>H<sub>5</sub>CO, which is formed by an abstraction of a hydrogen atom from the -CHO group in propanal, generates ethyl radicals (reaction 25) at a rate that is ~40 times faster than that of reaction 1. It is the ratio of the rates at which C<sub>2</sub>H<sub>5</sub>CO produces ethyl and methyl radicals (approximately 100) that determines the ratio of ethylene to methane. The values given in Table III do reproduce the experimental results in terms of the absolute values and the ratios as can readily be seen in Figures 7-9.

Although the reactions of the C<sub>2</sub>H<sub>5</sub>CO radical determine the concentration of ethyl and hence that of ethylene, this is not reflected in the sensitivity analysis (Figure 10). A factor of 5

change in  $k_{25}$  and  $k_{-25}$  has almost no effect on the concentration of ethylene. This is because the rate at which the radical C<sub>2</sub>H<sub>5</sub>CO decomposes is determined by the rate of its formation by abstractions. On the other hand, reaction 26 is endothermic ( $\Delta H_{26} = 29.05 \text{ kcal/mol}$ ) and the dissociation is slow. The production of methyl radicals and hence methane is therefore highly dependent on  $k_{26}$  as can readily be seen in Figure 10.

Figure 12 shows profiles of the main four reactive free radicals in the system, calculated at 1000 K. Ethyl radicals have the highest concentration; all reach a steady-state concentration after several hundred microseconds. Not included in this figure are isopropyl and *n*-propyl radicals whose concentrations are much smaller. Abstractions and dissociations in which these radicals participate affect the production rates of propylene and propane. The latter were found in very small concentrations in the postshock mixtures. As can be seen in Figure 13, the agreement for propylene, for example, is not at all satisfactory. We could not reduce the discrepancy between the experimental and calculated mole percent of propane and propylene unless unrealistic rate parameters

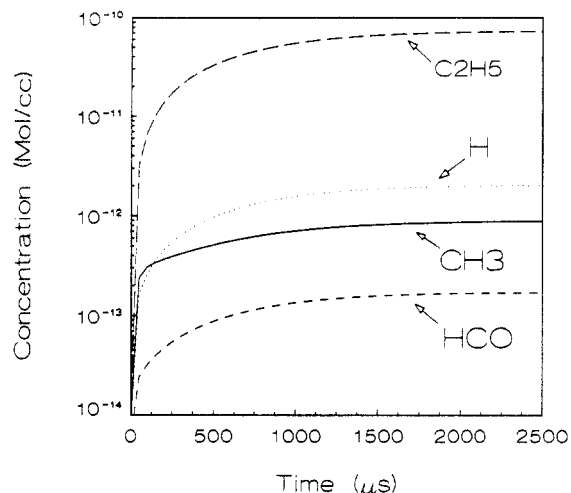


**Figure 12.** Profiles of four major reactive radicals in the system. The calculation is done for  $T_s = 1000$  K.

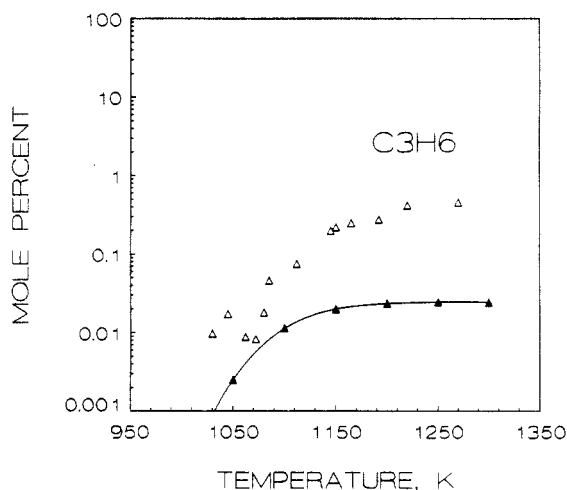


**Figure 13.** Comparison between experimental ( $\Delta$ ) and calculated ( $\blacktriangle$ ) mole percent of propylene. The agreement is not satisfactory.

were assigned to some of the reactions that are involved in the production of these species. This problem is still unsolved.

It is interesting to note that the product distribution obtained in the present experiment is very different from the one found in the low-temperature study.<sup>9</sup> In this study ethylene is the major reaction product whereas ethane is the major product at low

temperatures. The concentration ratio of these two substances is determined by the relative rates of decomposition to abstraction of the ethyl radical. This ratio is highly temperature dependent as the dissociation rate has some 40 kcal/mol activation energy whereas the abstraction has only several kilocalories per mole. A similar behavior has been observed in the high<sup>18,19</sup> and the low<sup>20,21</sup> temperature decomposition of propane.

A close look at the sensitivity analysis shows that some two-thirds of the reactions have very little or no effect at all on the production rate of any of the reaction products that are produced in the pyrolysis. These reactions in principle could be removed from the scheme since reduction of their rate constant by several orders of magnitude in another sensitivity study seemed to have no effect at all on the overall distribution. They were nevertheless left in the scheme as they may be expected to become important at different temperature and concentration ranges.

The question that always arises in studies of this type is to what extent the combination of rate parameters used in the study is unique. Is there another combination with a realistic rate parameter that can produce the same modeling results? In systems with relatively large number of products the interaction between the various elementary steps limits the freedom of arbitrary variation of rate parameters. Nevertheless some degrees of freedom are still left, and the correctness of the rate parameters must be supported by comparisons with other systems. We plan to study other similar systems in the future for this purpose.

### Conclusion

Production rates and distribution of products obtained in the thermal decomposition of propanal were accounted for with a kinetic scheme containing 52 elementary reactions and 22 species. The dissociation rates of unstable free radicals play a very important role in determining the concentrations and distribution of reaction products.

*Acknowledgment.* This work was supported by a grant from the U.S.-Israel Binational Science Foundation under Grant Agreement No. 84-00161. We thank Dr. Wing Tsang for helpful discussions.

**Registry No.**  $\text{CH}_3\text{CH}_2\text{CHO}$ , 123-38-6.

(18) Lifshitz, A.; Scheller, K.; Burcat, A. *Recent Developments in Shock Tube Research*, Proceedings of the Ninth International Shock Tube Symposium (1973); Bershader, D., Griffith, W., Eds.; Stanford University Press: Stanford, CA, 1973; p 690.

(19) Lifshitz, A.; Frenklach, M. *J. Phys. Chem.* **1975**, *79*, 686.

(20) Laidler, K. J.; Sagert; Wojciechowski, B. W. *Proc. R. Soc., Ser. A* **1962**, *270*, 242.

(21) Leathard, D. A.; Purnell, J. H. *Proc. R. Soc., Ser. A* **1968**, *305*, 517.